OIL/WATER FLOW IN A HORIZONTAL PIPE—DISPERSED FLOW REGIME

D.S. SANTOS[1], F.A.P. GARCIA[1], M.G. RASTEIRO[1] & P.M. FAIA[2]
[1] Chemical Process Engineering and Forest Products Research Centre (CIEPQPF), Department of Chemical Engineering, University of Coimbra, Portugal.
[2] Center of Mechanical Engineering, Materials and Processes (CEMMPRE), Electrical and Computers Engineering Department, University of Coimbra, Portugal.

ABSTRACT

In multiphase fluid flow, the formation of dispersed patterns, where one of the phases is completely dispersed in the other (continuous medium) is common, for example, in crude oil extraction, during the transport of water/oil mixture.

In this work, experimental and numerical studies were carried out for the flow of an oil/water mixture in a horizontal pipe, the dispersed liquid being a paraffin (oil with density 843 kg m^{-3} and viscosity 0.025 Pa s) and the continuous medium a water solution doped with NaCl (1000 μS. cm^{-1}). The tests were made for oil concentrations of 0.01, 0.13 and 0.22 v/v and velocities between 0.9 and 2.6 ms^{-1} of the mixture. Experimental work was performed in a pilot rig equipped with an electrical impedance tomography (EIT) system. Information on pressure drop, EIT maps, volumetric concentrations in the vertical diameter of the pipe and flow images were obtained. Simulations were performed in 2-dimensional geometry using the Eulerian–Eulerian approach and the k-ε model for turbulence modelling. The model was implemented in a computational fluid dynamics platform with the programme COMSOL Multiphysics version 5.3. The simulations were carried out using the Schiller–Neumann correlation for the drag coefficient and two equations for the viscosity calculation: Guth and Simba (1936) and Pal (2000). For the validation of the simulations, the pressure drop was the main control parameter.

The simulations predicted the fully dispersed flow patterns and the pressure drop calculated when using the Pal (2000) equation for the viscosity calculation showed the best fit. The results of the images of the flows obtained by the photographs and simulations were in good agreement.
Keywords: dispersed flow pattern, Euler–Euler model, oil/water flows, pressure drop.

1 INTRODUCTION

Multiphase flows in pipe occur in many industrial sectors and are most important in the petroleum industry. In petroleum extraction and production processes, oil transport occurs along with other materials (water, air and solid particles) [1]. Thus, depending on the materials transported, the flow can be biphasic (oil/water, water/air, air/solids, etc.), three-phase (air/water/solid, air/oil/solid, etc.) or multiphasic (more than three phases) [1–4]. The interaction between the fluids, when transported, leads to the formation of flow patterns, being the main ones classified as dispersed, stratified and intermittent [5]. In addition, the long distances that the fluids travel until reaching their destination demand very high energy costs [6]. Studies have been developed in the search for optimization and creation of fluid pumping systems that lead to the reduction of energy consumption. In the literature, experimental studies have been carried out to characterize the different types of flow [2], the presence of the waves at the interface [7, 8], the transition between flow patterns [9], among others. These studies involve filming of the flow, sampling techniques [5] and non-invasive techniques, such as some tomographic techniques. In the latter case, these techniques obtain information about the system through measurement of the electromagnetic, acoustic or electrical properties of the fluids [10–15]. In addition to the experimental studies, flow simulations have also been extensively developed. Numerical simulations have been performed using methods based on the solution of the transport equations for the fluids through the direct simulation of local and

ISSN: 2046-0546 (paper format), ISSN: 2046-0554 (online), http://www.witpress.com/journals
DOI: 10.2495/CMEM-V8-N2-123-134

instantaneous equations, such as level-set method [16–18], phase-field method [19, 20] or volume of fluids method [20, 21], or through the solution of the average equations. In the latter case, the systems can be modelled using a homogeneous model, where the phases are treated as pseudofluids with average properties, and in this approach, the flow pattern is treated in a less detailed way [22], through a Lagrangian–Eulerian approach, where one of the phases is treated from an Eulerian perspective (as in the single phase flow) and the other phase receives a Lagrangian treatment [23, 24], or using an Eulerian–Eulerian approach, where each phase is treated continuously and the coupling between the phases occurs through interfacial terms [25–27].

In this work, a numerical simulation study was developed to describe the dispersed oil/water flow in a horizontal pipe (length of 11.5 m and an internal diameter of 0.11 m) and another experimental study to validate the simulations. For the simulation, a Eulerian–Eulerian approach was used in conjunction with the Reynolds-averaged Navier–Stokes (RANS) equations and the k-ε turbulence model implemented in COMSOL Multiphysics 5.3. In the experimental study, electrical impedance tomography (EIT) was used to identify the flow pattern and to determine the distribution of the phases within the pipe. Simulation validation was performed by comparing the pressure drop data.

2 EXPERIMENTAL SETUP

The experimental tests for the oil/water dispersed flow were performed in a pilot plant rig (see Fig. 1).

The test fluids were liquid paraffin (density of 843±1 kg m^{-3} and viscosity of 0.025±0.0002 Pa s) and water saline solution doped with NaCl (to allow a higher contrast between the phases in the EIT images), the interfacial tension is 46.0±0.1 mN m. The tests were performed for mixtures with oil concentrations of 0.01, 0.13 and 0.22 v/v and velocities between 0.9 and 2.6 m s^{-1}, in a straight section of the rig with length of 11.5 m and internal diameter of 0.11 m. The experiments were carried out at constant temperature. Data on

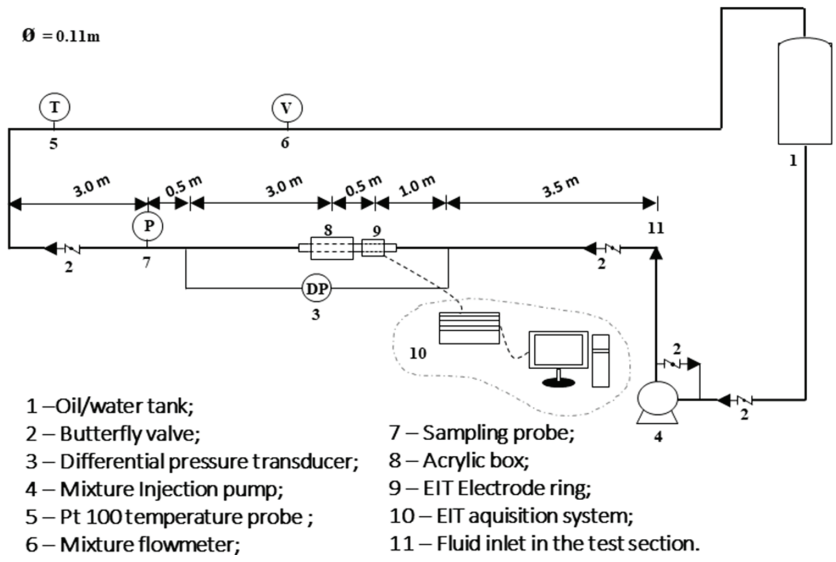

Figure 1: Scheme of the closed-loop pipeline.

pressure drop, flow rate, temperature, samples of the mixture along the vertical radius of the pipe and crude data of the EIT were collected.

For the EIT system, a ring with 32 titanium electrodes, 5 mm in diameter, circumferentially and equally spaced, inserted in the acrylic tube, was used (a more comprehensive description can be found in [13, 28]). Tests were done with an excitation frequency of 60 kHz, with 2 V peak-to-peak amplitude, and acquiring 1000 frames per second. In this manuscript, the opposite injection and measuring protocols were used. For the reconstruction of the images, the open software EIDORS was used off-line [29].

3 MATHEMATICAL MODEL DESCRIPTION

In this work a Euler–Euler strategy was considered. Assuming that there is no mass transfer and that both phases are incompressible, the continuity equations for the continuous phase, eqn (1), and dispersed, eqn (2), are

$$\frac{\partial\left(\rho_c \alpha_c\right)}{\partial t} + \nabla.\left(\rho_c \alpha_c u_c\right) = 0 \tag{1}$$

$$\frac{\partial\left(\rho_d \alpha_d\right)}{\partial t} + \nabla.\left(\rho_d \alpha_d u_d\right) = 0 \tag{2}$$

The volume fractions are assumed to be continuous functions and their sum is equal to one $\alpha_c = 1 - \alpha_d$, where ρ is the density, α is the volumetric fraction, t is the time, u is the velocity and the subscripts c and d correspond, respectively, to the continuous and the dispersed phases.

The equations for the momentum balance for the continuous phase, eqn (3), and dispersed, eqn (4), are presented below [17]:

$$\rho_c \alpha_c \left[\frac{\partial}{\partial t}\left(u_c\right) + u_c \nabla.\left(u_c\right)\right] = -\alpha_c \nabla P + \nabla.\left(\alpha_c \tau_c\right) + \alpha_c \rho_c g + F_{m,c} \tag{3}$$

$$\rho_d \alpha_d \left[\frac{\partial}{\partial t}\left(u_d\right) + u_d \nabla.\left(u_d\right)\right] = -\alpha_d \nabla P + \nabla.\left(\alpha_d \tau_d\right) + \alpha_d \rho_d g + F_{m,d} \tag{4}$$

where F_m. is the term for the interfacial momentum transfer, P is the pressure, g is gravity and τ is the viscous stress tensor.

In this model, the fluid phases are considered Newtonian in both equations and the viscous tensors for each phase can be written as

$$\tau_c = \mu_c \left(\nabla u_c + \left(\nabla u_c\right)^T - \frac{2}{3}\left(\nabla.u_c\right)^I\right) \tag{5}$$

$$\tau_d = \mu_c \left(\nabla u_d + \left(\nabla u_d\right)^T - \frac{2}{3}\left(\nabla.u_d\right)^I\right) \tag{6}$$

In this work, two viscosity models were used to predict thrheological behaviour of dispersed system:

Guth and Simba (1936) model—this model considers the interaction between droplets and can be used for a wider range of dispersed phase concentrations [30, 31].

$$n_r = 1 + 2.5\alpha_d + 14.1\alpha_d^2 \tag{7}$$

where n_r. is the relative viscosity given by

$$n_r = \frac{\mu}{\mu_d} \tag{8}$$

Pal (2000) model—proposes an empirical equation based on experimental data for the viscosity of different emulsion systems, covering a wide range of the viscosity ratio between dispersed phase and continuous phase, 4.1×10^{-3} to 1.17×10^{3} [32]:

$$n_r^{-2.5}\left[\frac{2n_r + 5b}{2 + 5b}\right]^{-2.5} = 1 - b_0\alpha_d \tag{9}$$

where b is the viscosity ratio between the continuous and the dispersed phases. Regarding b_0, if no experimental data is available, the parameter becomes equal to 1.35.

The drag force for the dispersed flow can be defined as

$$F_{drag,c} = F_{drag,d} = \beta u_s \tag{10}$$

$$\beta = \frac{3\alpha_d \rho_c C_d}{4\varnothing_d}|u_s| \tag{11}$$

where $F_{drag,c}$ is the drag force for the continuous phase, $F_{drag,d}$ the drag force for the dispersed phase, β is the sliding force coefficient, $\varnothing_d$ is the droplet diameter, C_d. is the drag coefficient for the diluted flow and u_s is the slip velocity between phases and is given by

$$u_s = u_d - u_c \tag{12}$$

The drag coefficient was calculated by the Schiller–Neumann correlation [33]:

$$C_D = \begin{cases} \dfrac{24}{Re_p}\left(1 + 0.15Re_p^{0.687}\right) Re_p < 1000 \\ 0.44\, Re_p > 1000 \end{cases} \tag{13}$$

where Re_p is the Reynolds of the particle and can be defined as

$$Re_p = \frac{\varnothing_d \rho_c |u_s|}{\mu_c} \tag{14}$$

Turbulence model

In this work, the RANS method was used to model turbulent flows. So, in this approach all time-dependent functions are expressed as the sum of a temporal mean and a floating component. The closing equation for the turbulent viscosity is given by [27]

$$\mu_T = \rho C_\mu \frac{k^2}{\varepsilon} \tag{15}$$

where C_μ is an experimentally obtained constant.

4 RESULTS AND DISCUSSION

For the simulations, the following hypotheses were applied: steady state, turbulent flow, incompressible, isothermal and without mass transfer between phases. The following input values were required: the tube wall roughness (10^{-4} m), the fluid inlet velocities, the volumetric oil concentration, the fluid properties and the droplet diameter (120 μm). The boundary conditions used for the simulations were the velocities of the mixture at the inlet, zero pressure at the outlet and no slip at the wall.

4.1 Geometry and mesh

The geometry and meshes were implemented using the COMSOL Multiphysics® program. Mesh independency studies were conducted for a volumetric oil concentration of 0.01 and velocity of the mixture of 0.9 ms^{-1}. The best mesh (pressure drop independent of further refinement) corresponded to 91371 elements. So, the number of elements of the mesh used in the simulations for a 2D geometry was 91371.

In this study, the simulations compare the results of the tests obtained using two different equations for the viscosity calculation: Guth and Simba (1936) and Pal (2000).

4.2 Pressure drop

In Fig. 2, graphs of pressure drop versus velocity of the mixture for the oil concentrations of 0.01, 0.13 and 0.22 v/v and for simulations performed using the equations of Guth and Simba (1936) (a) and Pal (2000) (b), for the calculation of viscosity are presented.

It is observed that for the lower velocities of the mixture, the two equations presented close values, similar to the experimental ones. However, the increase in velocity led the Guth and Simba equation (1936) to obtain values of pressure drop that are further away from the experimental ones, what was not observed for the equation of Pal (2000). In Tables 1–3, we find the experimental and simulated pressure drop values. Pressure drop was obtained for volumetric concentrations of 0.01 (Table 1), 0.13 (Table 2) and 0.22 (Table 3), and for mixing velocities between 0.9 and 2.6 m s^{-1}. The results show that the viscosity equation for the mixture has relevant influence on the values of pressure drop.

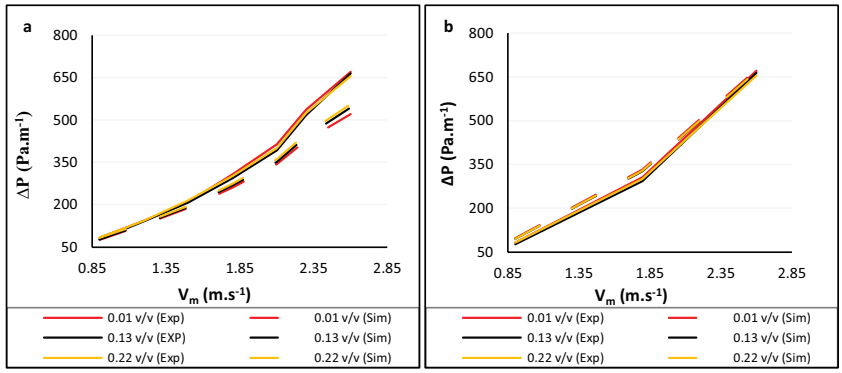

Figure 2: Pressure drop versus velocity of the mixture. Viscosity calculated by (a) the Guth and Simba (1936) equation and (b) the Pal (2000) equation.

Table 1: Experimental and simulated pressure drop values (ΔP) for oil/water dispersed flow. For the simulations, the viscosity is calculated by the Guth and Simba (1936) and Pal (2000) equations. Oil concentration of 0.01 v/v.

		Schiller–Neumann			
V_m	ΔP_{Exp}	Guth and Simba (1936) (Pa s)		Pal (2000) (Pa s)	
(ms^{-1})	($Pa\ m^{-1}$)	ΔP_{Sim} ($Pa\ m^{-1}$)	Error (%)	ΔP_{Sim} ($Pa\ m^{-1}$)	Error (%)
0.9	83.3	75.7	9.7	97.7	16.6
1.2	143.9	129.1	10.3	-	-
1.5	210.1	187.3	10.6	-	-
1.8	307.6	260.6	15.2	332.2	8.1
2.1	414.1	343.3	17.1	-	-
2.3	536.9	427.8	20.3	-	-
2.6	671.1	513.9	23.4	676.0	0.7

Table 2: Experimental and simulated pressure drop values (ΔP) for oil/water dispersed flow. For the simulations, the viscosity is calculated by the Guth and Simba (1936) and Pal (2000) equations. Oil concentration of 0.13 v/v.

		Schiller-Neumann			
V_m	ΔP_{Exp}	Guth and Simba (1936) (Pa s)		Pal (2000) (Pa s)	
(ms^{-1})	($Pa\ m^{-1}$)	ΔP_{Sim} ($Pa\ m^{-1}$)	Error (%)	ΔP_{Sim} ($Pa\ m^{-1}$)	Error (%)
0.9	77.3	77.7	0.5	97.0	25.4
1.2	141	132.3	6.2	-	-
1.5	206.8	192.5	6.9	-	-
1.8	293.2	267	8.9	328.0	11.8
2.1	393.2	352	10.4	-	-
2.3	516.3	441.3	14.5	-	-
2.6	664.5	543.8	18.1	670.1	0.8

Table 3: Experimental and simulated pressure drop values (ΔP) for oil/water dispersed flow for the simulations, the viscosity is calculated by the Guth and Simba (1936) and Pal (2000) equations. Oil concentration of 0.22 v/v.

		Schiller–Neumann			
V_m	ΔP_{Exp}	Guth and Simba (1936) (Pa s)		Pal (2000) (Pa s)	
($m\ s^{-1}$)	($Pa\ m^{-1}$)	ΔP_{Sim} ($Pa\ m^{-1}$)	Error (%)	ΔP_{Sim} ($Pa\ m^{-1}$)	Error (%)
0.9	83.6	83.8	0.2	97.0	16.0
1.2	142.7	135.5	5.3	-	-

1.5	214.5	196.5	8.4	-	-
1.8	301.6	273.1	9.4	328.5	8.9
2.1	400.8	360.4	10.1	-	-
2.3	523.9	451.4	13.8	-	-
2.6	654.6	556	15.1	670.1	2.4

4.3 Concentration profiles

In Figs. 3–5 the reconstructed images for oil concentrations of 0.01, 0.13 and 0.22 v/v, and mixture velocities of 0.9, 1.5, 2.1 and 2.6 ms^{-1} are presented. For the representation of the variation of the normalized conductivity, a colour system was used, where the red and blue colours indicate the normalized conductivity values for the pure oil and aqueous phases, respectively, and the variation between both colours, corresponds to the mixtures between the two phases. The normalization is done using the reference measurements for the 1000 $\mu S.\ cm^{-1}$ NaCl solution without oil. η is the normalized conductivity, σ_m is the conductivity of the mixture and σ_o is the reference conductivity:

$$\eta = \frac{\sigma_m - \sigma_o}{\sigma_0} \tag{16}$$

In the EIT images, it was not possible to distinguish the oil droplets because of their small size, but a homogeneous pattern was observed for all situations tested, confirming the existence of a dispersed flow pattern. However, as the oil concentration increased, the patterns

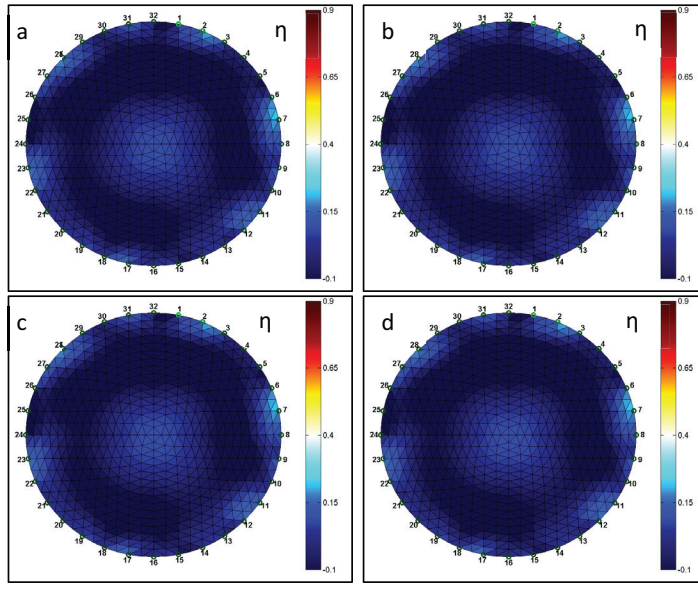

Figure 3: EIT images for oil/water dispersed flow. Oil concentration of 0.01 v/v and velocities of the mixture: (a) 0.9 ms^{-1}, (b) 1.5 ms^{-1}, (c) 2.1 ms^{-1} and (d) 2.6 ms^{-1}.

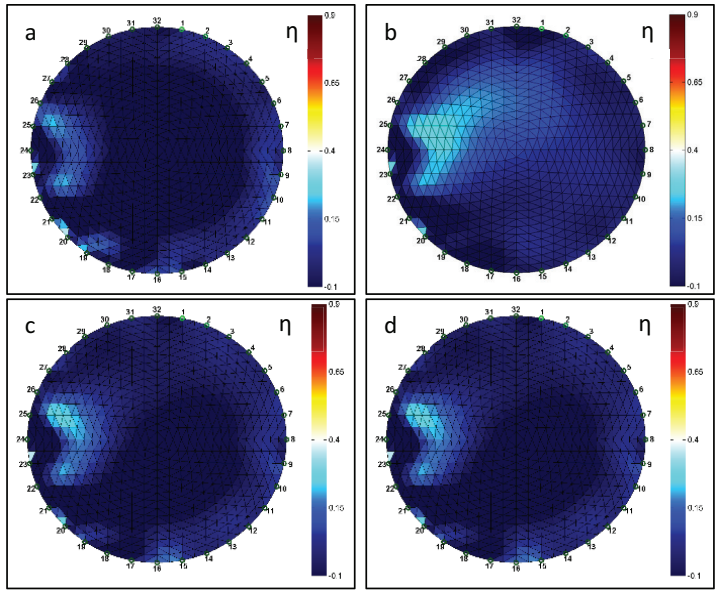

Figure 4: EIT images for oil/water dispersed flow. Oil concentration of 0.13 v/v and velocities of the mixture (a) 0.9 ms^{-1}, (b) 1.5 ms^{-1}, (c) 2.1 ms^{-1} and (d) 2.6 ms^{-1}.

became more heterogeneous (Figs. 4 and 5), with a higher predominance of the light blue colour (oil/water mixture) when the oil concentration increased.

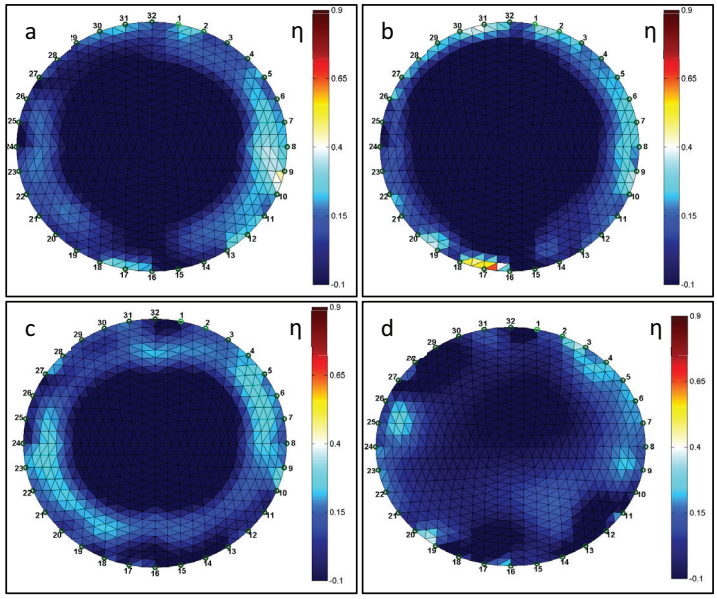

Figure 5: EIT images for oil/water dispersed flow. Oil concentration of 0.22 v/v and velocities of the mixture: (a) 0.9 ms^{-1}, (b) 1.5 ms^{-1}, (c) 2.1 ms^{-1} and (d) 2.6 ms^{-1}.

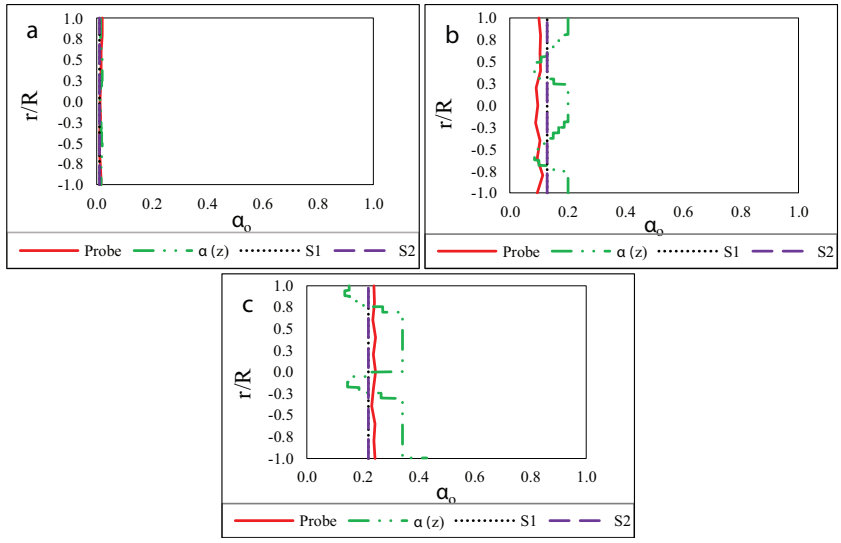

Figure 6: Radial profile of the oil volumetric concentration (1D) for oil/water dispersed flow. Velocity of the mixture of 0.9 m s^{-1} and oil concentration of (a) 0.01 v/v, (b) 0.13 v/v and (c) 0.22 v/v. In the simulations, (S1) corresponds to the Guth and Simba (1936) equation and (S2) to the Pal (2000) equation.

In Figs. 6 and 7, the volumetric oil concentration radial profiles (1D) obtained by the sampling/pycnometry and EIT and through the simulations are presented. Those profiles

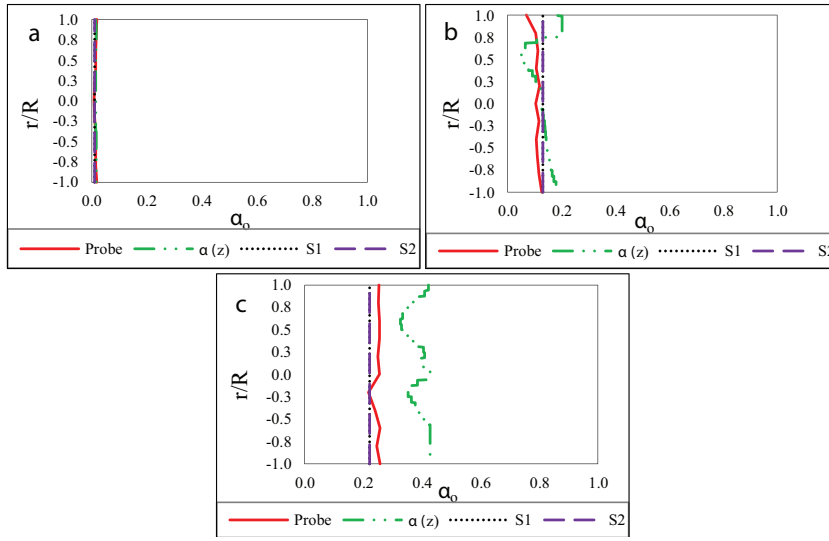

Figure 7: Radial profile of the oil volumetric concentration (1D) for oil/water dispersed flow. Velocity of the mixture of 2.6 m s^{-1} and oil concentration of (a) 0.01 v/v, (b) 0.13 v/v and (c) 0.22 v/v. In the simulations, (S1) corresponds to the Guth and Simba (1936) equation and (S2) to the Pal (2000) equation.

correspond to oil concentrations of 0.01, 0.13 and 0.22 v/v and to the velocities of the mixture of 0.9m s^{-1} (Fig. 6) and 2.6 ms^{-1} (Fig. 7). In the case of the EIT technique, the normalized conductivity profiles were converted to volumetric concentrations of the oil using a methodology that calculates the oil concentration ($\alpha(z)$) through the ratio of the volumetric concentration of the oil (α_0) to a control area along the radius (A_σ) multiplied by the normalized conductivity (η) eqn (16) [13]:

$$a(z) = \frac{\alpha_0}{A\sigma}\eta \tag{17}$$

The concentration profiles of the oil (EIT) show, for the oil concentration of 0.01 v/v, agreement with the profiles obtained through pycnometry. For the oil concentration of 0.13 v/v, the EIT profiles presented also reasonable agreement. Finally, for the oil concentration of 0.22 v/v, the concentration profiles presented overestimated results, comparing with the data obtained by the probe, for the highest velocity. As for the simulated profiles, (S1) corresponding to the Guth and Simba (1936) equation and (S2) to the Pal (2000) equation, the profiles are identical independently of the equation used, and were able to predict the experimental results satisfactorily.

5 CONCLUSIONS

In this work, the experimental tests were able to reproduce the dispersed flow pattern for three volumetric oil concentrations and for a range of velocities of the mixture, in a horizontal pipe, from 0.9 to 2.6 ms^{-1}, while using liquid paraffin to mimic the crude oil. The dispersed flow regime was confirmed using the EIT technique.

The best fit between the simulated and experimental values of pressure drop was obtained using the equation of Pal (2000) for the mixture viscosity and the Schiller–Neumann correlation for drag coefficient.

Regarding the 1D radial profiles, EIT agreed reasonably well with the data obtained through sampling/pycnometry, except for the highest concentration and velocity. In general, the 1D simulated oil concentration profiles agreed well with the experimental radial volumetric oil concentration profiles, obtained by sampling and pycnometry.

ACKNOWLEDGEMENTS

This work was conducted during a scholarship supported by the International Cooperation Program CAPES/COFECUB, financed by CAPES – Brazilian Federal Agency for Support and Evaluation of Graduate Education (BEX: 9270/13-2). We also acknowledge the financial support of the Portuguese Foundation for Science and Technology (PEST – UI102 – 2013).

REFERENCES

[1] Rodriguez, O.M.H., *Escoamento Multifásico*, ABCM—Associação Brasileira de Engenharia e Ciências Mecânica, Rio de Janeiro, Brasil, 2011.

[2] Trallero, J.L., Sarica, C. & Brill, J.P., A study of oil-water flow patterns in horizontal pipes. *SPE Production & Facilities*, **12**(**3**), pp. 165–172, 1997. https://doi.org/10.2118/36609-pa

[3] Tan, C., Wu, H. & Dong, F., Horizontal oil–water two-phase flow measurement with information fusion of conductance ring sensor and cone meter. *Flow Measurement and Instrumentation*, **34**, pp. 83–90, 2013. https://doi.org/10.1016/j.flowmeasinst.2013.08.006

[4] Grassi, B., Strazza, D. & Poesio, P., Experimental validation of theoretical models in two-phase high-viscosity ratio liquid–liquid flows in horizontal and slightly inclined

pipes. *International Journal of Multiphase Flow*, **34**(**10**), pp. 950–965, 2008. https://doi.org/10.1016/j.ijmultiphaseflow.2008.03.006

[5] Wang, W., Gong, J. & Angeli, P., Investigation on heavy crude-water two phase flow and related flow characteristics. *International Journal of Multiphase Flow*, **37**(**9**), pp. 1156–1164, 2011. https://doi.org/10.1016/j.ijmultiphaseflow.2011.05.011

[6] Rodriguez, O.M.H. & Baldani, L.S., Prediction of pressure gradient and holdup in wavy stratified liquid–liquid inclined pipe flow. *Journal of Petroleum Science and Engineering*, **96–97**, pp. 140–151, 2012. https://doi.org/10.1016/j.petrol.2012.09.007

[7] Al-Wahaibi, T. & Angeli, P., Experimental study on interfacial waves in stratified horizontal oil–water flow. *International Journal of Multiphase Flow*, **37**(**8**), pp. 930–940, 2011. https://doi.org/10.1016/j.ijmultiphaseflow.2011.04.003

[8] Rodriguez, O.M. & Castro, M.S., Interfacial-tension-force model for the wavy-stratified liquid–liquid flow pattern transition. *International Journal of Multiphase Flow*, **58**, pp. 114–126, 2014. https://doi.org/10.1016/j.ijmultiphaseflow.2013.09.003

[9] Al-Wahaibi, T., Yusuf, N., Al-Wahaibi, Y. & Al-Ajmi, A., Experimental study on the transition between stratified and non-stratified horizontal oil–water flow. *International Journal of Multiphase Flow*, **38**(**1**), pp. 126–135, 2012. https://doi.org/10.1016/j.ijmultiphaseflow.2011.08.007

[10] Wang, M., *Industrial Tomography: Systems and Applications*, Elsevier, MA. Boston, 2015.

[11] Ismail, I., Gamio, J.C., Bukhari, S.A. & Yang, W.Q., Tomography for multi-phase flow measurement in the oil industry. *Flow Measurement and Instrumentation*, **16**(**2–3**), pp. 145–155, 2005. https://doi.org/10.1016/j.flowmeasinst.2005.02.017

[12] Hasan, N.M. & Azzopardi, B.J., Imaging stratifying liquid–liquid flow by capacitance tomography. *Flow Measurement and Instrumentation*, **18**(**5–6**), pp. 241–246, 2007. https://doi.org/10.1016/j.flowmeasinst.2007.07.007

[13] Silva, R., Garcia, F.A.P., Faia, P. M., Krochak, P., Söderberg, D., Lundell, F. & Rasteiro, M.G., Validating dilute settling suspensions numerical data through MRI, UVP and EIT measurements. *Flow Measurement and Instrumentation*, **50**, pp. 35–48, 2016. https://doi.org/10.1016/j.flowmeasinst.2016.06.003

[14] Che, H.Q., Wu, M., Ye, J.M., Yang, W.Q. & Wang, H.G., Monitoring a lab-scale wurster type fluidized bed process by electrical capacitance tomography. *Flow Measurement and Instrumentation,* **62**, pp. 223–34, 2017. https://doi.org/10.1016/j.flowmeasinst.2017.09.005

[15] Vauhkonen, M., *Electrical Impedance Tomography and Prior Information*, University of Kuopio, Kuopio, Finland, 1997.

[16] Bilger, C., Aboukhedr, M., Vogiatzaki, K. & Cant, R.S., Evaluation of two-phase flow solvers using level set and volume of fluid methods. *Journal of Computational Physics*, **345**, pp. 665–686, 2017. https://doi.org/10.1016/j.jcp.2017.05.044

[17] Yap, Y.F., Li, H.Y., Lou, J., Pan, L.S. & Shang, Z., Numerical modeling of three-phase flow with phase change using the level-set method. *International Journal of Heat and Mass Transfer*, **115**, pp. 730–740, 2017. https://doi.org/10.1016/j.ijheatmasstransfer.2017.08.076

[18] Olsson, E. & Kreiss, G., A conservative level set method for two phase flow. *Journal of Computational Physics*, **210**(**1**), pp. 225–246, 2005. https://doi.org/10.1016/j.jcp.2005.04.007

[19] Alam, J.M., A wavelet based numerical simulation technique for two-phase flows using the phase field method. *Computers & Fluids*, **146**, pp. 143–153, 2017. https://doi.org/10.1016/j.compfluid.2017.01.015

[20] Zhao, J., Wang, Q. & Yang, X., Numerical approximations to a new phase field model for two phase flows of complex fluids. *Computer Methods in Applied Mechanics and Engineering*, **310**, pp. 77–97, 2016. https://doi.org/10.1016/j.cma.2016.06.008

[21] Pozzetti, G. & Peters, B., A multiscale DEM-VOF method for the simulation of three-phase flows. *International Journal of Multiphase Flow*, **99**, pp. 186–204, 2018. https://doi.org/10.1016/j.ijmultiphaseflow.2017.10.008

[22] Arunkumar, S., Adhavan, J., Venkatesan, M., Das, S.K. & Balakrishnan, A.R., Two phase flow regime identification using infrared sensor and volume of fluids method. *Flow Measurement and Instrumentation*, **51**, pp. 49–54, 2016. https://doi.org/10.1016/j.flowmeasinst.2016.08.012

[23] Angeli, P. & Hewitt, G.F., Pressure gradient in horizontal liquid–liquid flows. *International Journal of Multiphase Flow*, **24**(**7**), pp. 1183–1203, 1999. https://doi.org/10.1016/s0301-9322(98)00006-8

[24] Schillings, J., Doche, O., Tano Retamales, M., Bauer, F., Deseure, J. & Tardu, S., Four-way coupled Eulerian–Lagrangian direct numerical simulations in a vertical laminar channel flow. *International Journal of Multiphase Flow*, **89**, pp. 92–107, 2017. https://doi.org/10.1016/j.ijmultiphaseflow.2016.10.006

[25] Sommerfeld, M., Van Wachem, B. & Oliemans, R. (eds), *Best Practice Guidelines for Computational Fluid Dynamics of Dispersed Multi-Phase Flows*, European Research Community on Flow, Turbulence and Combustion (ERCOFTAC), Brüssel.

[26] Kartushinsky, A., Tisler, S., Oliveira, J.L.G. & van der Geld, C.W.M., Eulerian-Eulerian modelling of particle-laden two-phase flow. *Powder Technology*, **301**, pp. 999–1007, 2016. https://doi.org/10.1016/j.powtec.2016.07.053

[27] Almohammed, N., Alobaid, F., Breuer, M., and Epple, B., A comparative study on the influence of the gas flow rate on the hydrodynamics of a gas–solid spouted fluidized bed using Euler–Euler and Euler–Lagrange/DEM models. *Powder Technology*, **264**, pp. 343–364, 2014. https://doi.org/10.1016/j.powtec.2014.05.024

[28] Faia, P.M., Silva, R., Rasteiro, M.G., Garcia, F.A.P., Ferreira, A.R., Santos, M.J., Santos, J.B. & Coimbra, A.P., Imaging particulate two-phase flow in liquid suspensions with electric impedance tomography. *Particulate Science and Technology*, **30**(**4**), pp. 329–342, 2012. https://doi.org/10.1080/02726351.2011.575444

[29] Polydorides, N. & Lionheart, W.R.B., A matlab toolkit for three-dimensional electrical impedance tomography: A contribution to the Electrical Impedance and Diffuse Optical Reconstruction Software project. *Measurement Science and Technology*, **13**(**12**), pp. 1871–1883, 2002, https://doi.org/10.1088/0957-0233/13/12/310

[30] Pouraria, H., Seo, J.K. & Paik, J.K., Numerical modelling of two-phase oil–water flow patterns in a subsea pipeline. *Ocean Engineering*, **115**, pp. 135–148, 2016, https://doi.org/10.1016/j.oceaneng.2016.02.007

[31] Walvekar, R.G., Choong, T.S., Hussain, S.A., Khalid, M. & Chuah, T.G., Numerical study of dispersed oil–water turbulent flow in horizontal tube. *Journal of Petroleum Science and Engineering*, **65**(**3–4**), pp. 123–128, 2009. https://doi.org/10.1016/j.petrol.2008.12.019

[32] Xu, X.X., Study on oil–water two-phase flow in horizontal pipelines. *Journal of Petroleum Science and Engineering*, **59**(**1**), pp. 43–58, 2007. https://doi.org/10.1016/j.petrol.2007.03.002

[33] Liu, Z. & Li, B., Scale-adaptive analysis of Euler-Euler large eddy simulation for laboratory scale dispersed bubbly flows. *Chemical Engineering Journal*, **338**, pp. 465–477, 2018. https://doi.org/10.1016/j.cej.2018.01.051